

# Single-sided Marchenko focusing of compressional and shear waves

Kees Wapenaar\*

*Department of Geoscience and Engineering, Delft University of Technology, 2600 GA Delft, The Netherlands*

(Received 5 August 2014; revised manuscript received 3 October 2014; published 11 December 2014)

In time-reversal acoustics, waves recorded at the boundary of a strongly scattering medium are sent back into the medium to focus at the original source position. This requires that the medium can be accessed from all sides. We discuss a focusing method for media that can be accessed from one side only. We show how complex focusing functions, emitted from the top surface into the medium, cause independent foci for compressional and shear waves. The focused fields are isotropic and act as independent virtual sources for these wave types inside the medium. We foresee important applications in nondestructive testing of construction materials and seismological monitoring of processes inside the Earth.

DOI: [10.1103/PhysRevE.90.063202](https://doi.org/10.1103/PhysRevE.90.063202)

PACS number(s): 43.20.+g, 43.40.Sk, 91.30.-f

## I. INTRODUCTION

In the field of time-reversal acoustics [1], waves that are recorded at the boundary of a medium are, after time-reversal, sent back into the medium to focus at the original source position (Fig. 1). A favorable aspect is that, in strongly scattering media, the backpropagated multiply scattered waves contribute significantly to the resolution of the focal spot [2,3]. The time-reversal principle applies to any kind of wave field that is governed by a time-symmetric wave equation. Hence, apart from acoustic waves in lossless media, it also holds for electromagnetic [4] and elastodynamic waves [5,6] in lossless media. For example, time-reversed elastodynamic waves, sent back into the medium, focus at the original source position after an intricate interplay of backpropagating multiply scattered and mode-converted waves.

An important underlying assumption of the time-reversal principle is that the boundary from which the wave field is sent back into the medium entirely encloses the medium (except that no sources are needed at perfectly reflecting parts of the boundary). In many practical situations the medium can be approached from one side only. This puts severe restrictions on the focusing aspects of the backpropagated field. The reason is that the interplay of backpropagating multiply scattered and mode-converted waves breaks down when a significant part of the wave field is missing.

For scalar (i.e., nonconverted) waves in a 1D medium, Rose [7,8] introduced a “single-sided” autofocusing method, which only requires the reflection response at one side of the medium as input. He showed that the focusing field to be emitted into the medium is a  $\delta$  pulse, followed by a solution of the Marchenko equation [9,10]. Broggin and Snieder [11] demonstrated that because the focused field is isotropic, it can be considered as a virtual source inside the medium, at the position of the focal point. They obtained the Green’s function of the unknown medium between the virtual source and the surface. A 3D extension of these concepts [12,13] has led to new imaging methodology for single-sided scalar reflection data [14,15].

In the next section we briefly review the time-reversal method for elastodynamic waves at the hand of a numerical

example using a layered medium and we indicate the limitations of this method for single-sided focusing. Next, we derive step-by-step a new Marchenko-type single-sided elastodynamic focusing method, which separately focuses compressional and shear waves at a focal point inside a layered medium. The focused fields act as independent virtual sources for compressional and shear waves inside the medium, of which the responses (the elastodynamic Green’s functions) are observed at the surface. We conclude by indicating how this single-sided elastodynamic focusing method can be generalized for 3D inhomogeneous media.

## II. TIME-REVERSAL METHOD

We review the elastodynamic time-reversal method and its limitations at the hand of the horizontally layered model of Fig. 2. The propagation velocities for compressional ( $P$ ) and shear ( $S$ ) waves are indicated by  $c_P$  and  $c_S$ , respectively; the mass density  $\rho$  is taken constant throughout the medium. The numbers along the depth ( $z$ ) axis represent arbitrary units (for example, “m” for shallow geophysical applications, or “tenths of mm” for ultrasonic applications). The half-spaces above and below the transparent boundaries at  $z_T = 0$  and  $z_B = 2800$  are homogeneous (subscripts  $T$  and  $B$  stand for top and bottom, respectively).

For horizontally layered media it is convenient to decompose wave fields into plane waves and analyze wave propagation per plane-wave component. We define the plane-wave decomposition of a space-dependent ( $x, z$ ) and time-dependent ( $t$ ) wavefield quantity  $u(x, z, t)$  as

$$u(p, z, \tau) = \int_{-\infty}^{\infty} u(x, z, \tau + px) dx. \quad (1)$$

Here  $p$  is the so-called rayparameter (or horizontal slowness) and  $\tau$  is a new time coordinate, usually called intercept time [16]. The relation with the more common plane-wave decomposition by Fourier transform becomes clear if we apply the temporal Fourier transform,

$$u(\omega) = \int_{-\infty}^{\infty} u(t) \exp(-j\omega t) dt \quad (2)$$

\*c.p.a.wapenaar@tudelft.nl

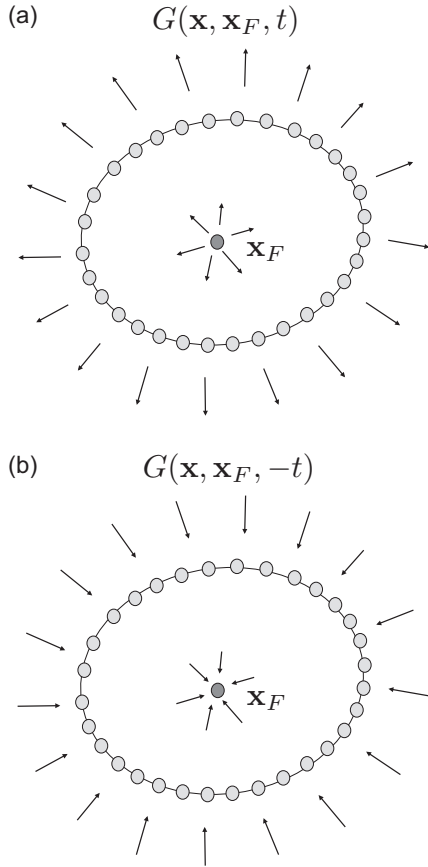


FIG. 1. Principle of time-reversal acoustics [1]. (a) The response to a source at  $\mathbf{x}_F$  is represented here by the Green's function  $G(\mathbf{x}, \mathbf{x}_F, t)$ . This response is observed at all  $\mathbf{x}$  at the boundary of the medium. (b) The time-reversed Green's function  $G(\mathbf{x}, \mathbf{x}_F, -t)$  is emitted from the boundary back into the medium and focuses at  $\mathbf{x}_F$ .

(with  $t$  replaced by  $\tau$ ), to both sides of Eq. (1). This gives

$$u(p, z, \omega) = \int_{-\infty}^{\infty} u(x, z, \omega) \exp(j\omega p x) dx. \quad (3)$$

Note that the right-hand side represents a spatial Fourier transform, with horizontal wavenumber  $k_x = \omega p$ . Each wavenumber  $k_x$  corresponds to a plane-wave component, of which the propagation angle  $\alpha$  obeys  $k_x = k \sin \alpha$ , with  $k = \omega/c$ , where  $c$  may stand for  $c_P$  or  $c_S$ . Hence,  $u(p, z, \omega)$  in Eq. (3), and consequently  $u(p, z, \tau)$  in Eq. (1), represents for each rayparameter  $p$  a plane wave component, with propagation angle  $\alpha$  obeying  $p = (\sin \alpha)/c$ .

We model the response to a source at  $z_F = 1800$  in the medium of Fig. 2. The plane-wave response can be obtained either by modeling the response to a point source and decomposing it into plane waves or by transforming the elastodynamic wave equation to the  $(p, z, \omega)$  domain, solving this equation per rayparameter  $p$ , and transforming the result back to the  $(p, z, \tau)$  domain. We follow the latter approach; see Ref. [17] for details. We choose a single rayparameter  $p = 0.0002$  s/m. In the layer containing the source, where  $c_P = 2500$  m/s and  $c_S = 1800$  m/s, this  $p$  value corresponds to  $P$  and  $S$  waves propagating under angles  $\alpha_P = 30^\circ$  and  $\alpha_S = 21^\circ$ , respectively. Figures 3(a) and 3(b) show the

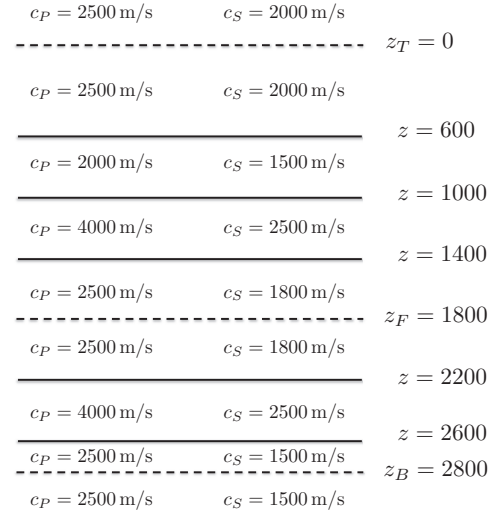


FIG. 2. Horizontally layered model.

responses to  $P$ - and  $S$ -wave sources, respectively, in the  $(p, z, \tau)$  domain for the chosen rayparameter  $p = 0.0002$  s/m. Here the horizontal axes denote intercept time ( $\tau$ ), displayed in arbitrary units (for example, “s” for shallow geophysics, or “tenths of ms” for ultrasonics). The right halves of the figures represent positive time ( $\tau > 0$ ). The figures show a superposition of flux-normalized  $P$  and  $S$  waves; superscripts + and – stand for downward and upward propagation, respectively. The relation between these flux-normalized quantities and the measurable wave fields is discussed in Appendix A. In Figs. 3(a) and 3(b) we clearly observe waves propagating away from the source at  $z_F = 1800$ . Note that  $P$  and  $S$  waves propagate under different angles in these  $(z, \tau)$  diagrams, as a result of the different propagation velocities.

In a time-reversal experiment, the wave fields recorded at the enclosing boundary are reversed in time and sent back into the medium from the enclosing boundary (Fig. 1). For a horizontally layered medium the “enclosing boundary” consists of the top and bottom boundaries, at depths  $z_T$  and  $z_B$ , respectively. In our example, the wave fields recorded at these boundaries are nothing but the first and last traces in Figs. 3(a) and 3(b). First, we take the time reversals of the first and last trace of Fig. 3(a), change the polarity of the  $S$ -wave parts, and send these waves back into the medium (actually, because this is a numerical experiment, we model the response of the layered medium to these incident waves). The result is shown in Fig. 4(a). The left half of the figure represents negative time ( $\tau < 0$ ). The  $\tau < 0$  parts of the top and bottom trace are the time-reversed responses that are sent back into the medium. The  $\tau < 0$  parts of the other traces show how the wave fields propagate through the medium, scatter at the interfaces, and at  $\tau = 0$  focus as  $P$  waves at the dot at  $z_F = 1800$  (the depth of the original source). The right half of the figure represents positive time ( $\tau > 0$ ). We see waves propagating away from the focal point at  $z_F = 1800$ , similar as in the  $P$ -wave source response in Fig. 3(a). Hence, the focal point acts as a virtual source for  $P$  waves and the response at positive time in Fig. 4(a) can be seen as the Green's function for a  $P$ -wave source, convolved with the  $P$ -wave source function.

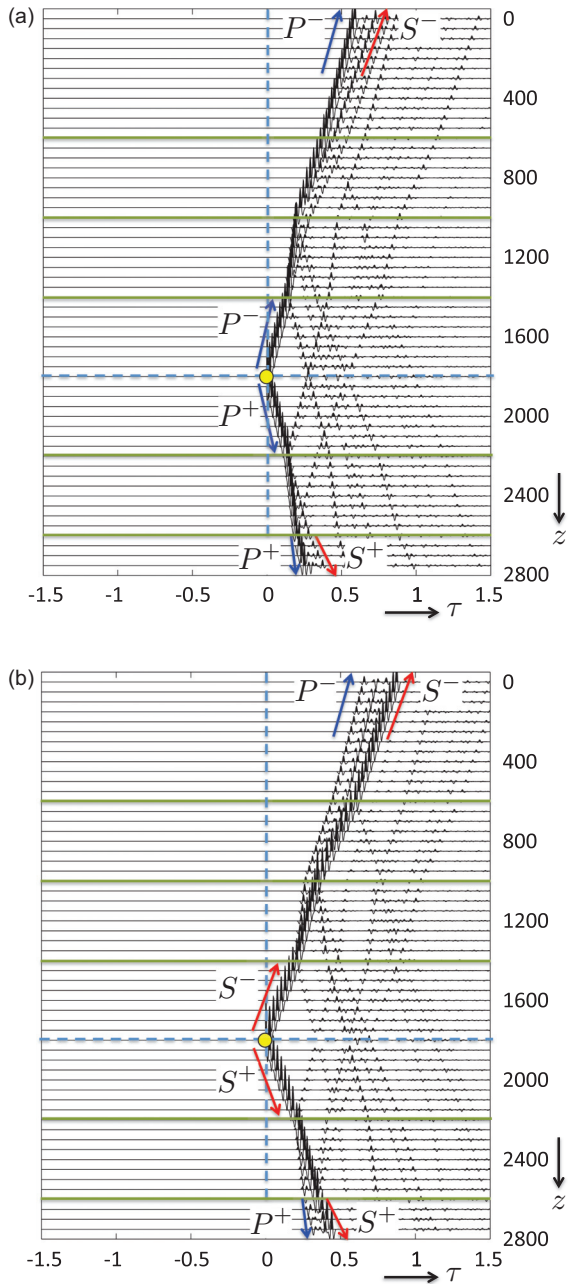


FIG. 3. (Color online) Forward modeled responses to  $P$ - and  $S$ -wave sources.

The relation between this type of Green’s function and the more common elastodynamic Green’s tensor is discussed in Appendix A. Next, we take the time-reversals of the first and last trace of Fig. 3(b), change the polarity of the  $P$ -wave parts, and send these waves back into the medium. The result is shown in Fig. 4(b). We see the waves focusing as  $S$  waves at  $z_F = 1800$  and propagating away from the focal point, similar as in the  $S$ -wave source response in Fig. 3(b). Hence, this time the focal point acts as a virtual source for  $S$  waves and its response can be seen as the Green’s function for an  $S$ -wave source, convolved with the  $S$ -wave source function.

Often the medium can be approached from one side only. This is illustrated in Fig. 5, where the same time-reversed

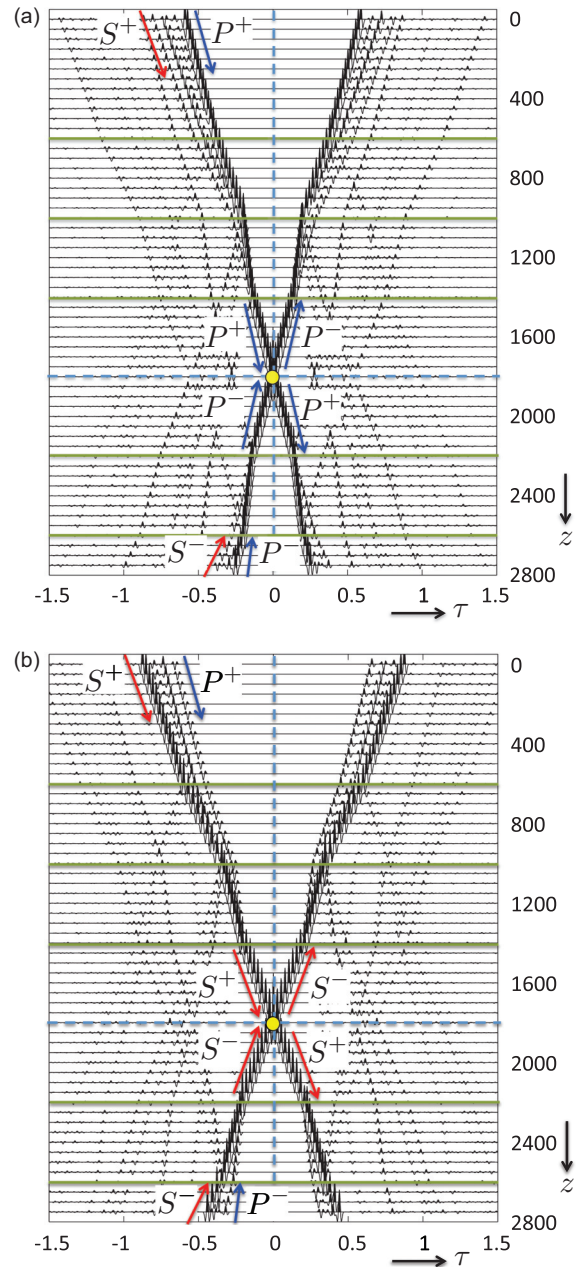


FIG. 4. (Color online) Time-reversal method: two-sided illumination.

fields as in Fig. 4 are emitted into the medium from above, but no fields are emitted from below. Note that at  $\tau = 0$  there is still a downgoing  $P$  wave [Fig. 5(a)] or a downgoing  $S$  wave [Fig. 5(b)] propagating through the focal depth  $z_F = 1800$ , but in addition there are many other events that degrade the focus quality. Moreover, there are no clear upgoing  $P$  or  $S$  waves propagating through the focal depth at  $\tau = 0$ . Hence, for single-sided accessible media another focusing approach is required.

Fink and coworkers [3,18,19] developed an iterative time-reversal scheme to improve the focusing in media, which are accessible from one side only. Their method focuses an acoustic wave field onto the strongest scatterers in the

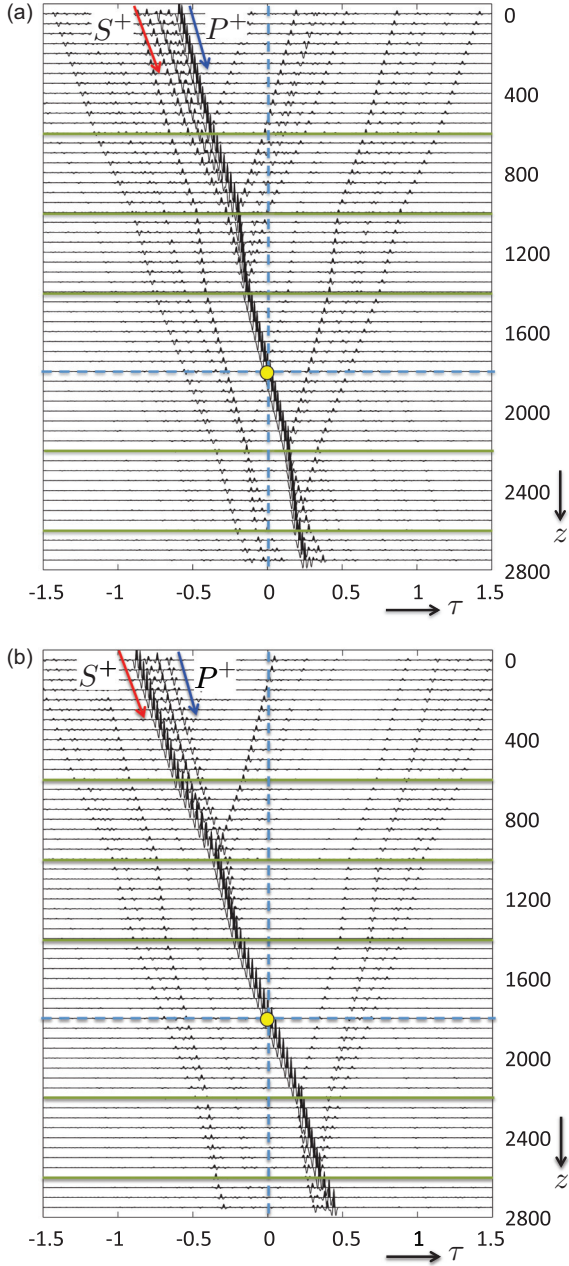


FIG. 5. (Color online) Time-reversal method: single-sided illumination.

medium. The 1D autofocusing method of Rose [7,8] and our 3D single-sided Marchenko focusing method [12,13] focus acoustic waves at any point inside a medium, thereby accounting for internal multiple scattering. The 3D method requires, apart from the measured reflection response of the medium, an estimate of the direct waves between the focal point and the acquisition surface. To the knowledge of the author, the iterative time-reversal method has not been extended for elastodynamic waves. Research to extending the Marchenko focusing method for elastodynamic wave fields has only started recently. Da Costa *et al.* [20–22] investigate an elastodynamic extension of Ref. [12] and illustrate with numerical experiments the advantages and limitations of their

approach. In a recent paper [23] we briefly introduce another approach to generalize the single-sided Marchenko method for elastodynamic waves and show that, at least in principle, all multiply scattered and mode-converted waves are properly taken into account. Here we discuss the latter approach more extensively and, in particular, carefully analyze its focusing properties. With a numerical example we show that with single-sided focusing functions, a focusing result can be obtained which is identical to the two-sided time-reversal result in Fig. 4.

### III. SINGLE-SIDED GREEN'S FUNCTION REPRESENTATION

Here we derive a representation for the elastodynamic Green's function for  $P$ - and  $S$ -wave sources at depth  $z_F$ , in terms of the single-sided reflection response at the top boundary  $z_T$ . Consider an arbitrary horizontally layered lossless medium below  $z_T$ ; the half-space above  $z_T$  is homogeneous. A downward propagating wavefield vector  $\mathbf{u}^+(p, z, \tau)$  is incident to this medium from above. Its response is an upward propagating wavefield vector  $\mathbf{u}^-(p, z, \tau)$ . These vectors contain downward and upward propagating plane  $P$  and  $S$  waves, as follows

$$\mathbf{u}^+ = \begin{pmatrix} P^+ \\ S^+ \end{pmatrix}(p, z, \tau) \quad \text{and} \quad \mathbf{u}^- = \begin{pmatrix} P^- \\ S^- \end{pmatrix}(p, z, \tau). \quad (4)$$

The relation between these wavefield vectors and measurable wavefield quantities is discussed in Appendix A. At  $z_T$  these wavefield vectors are related via

$$\mathbf{u}^-(p, z_T, \tau) = \int_{-\infty}^{\tau} \mathbf{R}(p, z_T, \tau - \tau') \mathbf{u}^+(p, z_T, \tau') d\tau', \quad (5)$$

where  $\mathbf{R}(p, z_T, \tau)$  is the reflection response matrix of the layered medium at the top boundary  $z_T$ . It is partitioned as follows:

$$\mathbf{R}(p, z_T, \tau) = \begin{pmatrix} R_{P,P} & R_{P,S} \\ R_{S,P} & R_{S,S} \end{pmatrix}(p, z_T, \tau). \quad (6)$$

Here  $R_{X,Y}(p, z_T, \tau)$  is the plane-wave reflection response at  $z_T$  in terms of upgoing  $X$  waves in response to downgoing  $Y$  waves (where each of the subscripts  $X$  and  $Y$  can stand for either  $P$  or  $S$ ). At an arbitrarily chosen depth level  $z_F$  (below  $z_T$ ) the response to  $\mathbf{u}^+(p, z_T, \tau)$  is denoted as  $\mathbf{u}^+(p, z_F, \tau)$  and  $\mathbf{u}^-(p, z_F, \tau)$ . These wavefield vectors are related to  $\mathbf{u}^+(p, z_T, \tau)$  via

$$\mathbf{u}^{\pm}(p, z_F, \tau) = \int_{-\infty}^{\tau} \mathbf{G}^{\pm,+}(p, z_F, z_T, \tau - \tau') \mathbf{u}^+(p, z_T, \tau') d\tau', \quad (7)$$

where  $\mathbf{G}^{\pm,+}(p, z_F, z_T, \tau)$  is a Green's matrix, which is partitioned in a similar way as the reflection response matrix  $\mathbf{R}(p, z_T, \tau)$ , hence

$$\mathbf{G}^{\pm,+}(p, z_F, z_T, \tau) = \begin{pmatrix} G_{P,P}^{\pm,+} & G_{P,S}^{\pm,+} \\ G_{S,P}^{\pm,+} & G_{S,S}^{\pm,+} \end{pmatrix}(p, z_F, z_T, \tau). \quad (8)$$

The second superscript of the Green's matrix (+) refers to the downward propagation direction at  $z_T$ , whereas the first superscript ( $\pm$ ) refers to the downward (+) or upward (−) propagation direction at  $z_F$ .

Next, we consider a reference medium, which is identical to the actual medium above  $z_F$  and reflection-free below  $z_F$ . We define a downward propagating focusing wavefield vector  $\mathbf{f}_p^+(p, z, \tau)$ , which is incident to this reference medium from the upper half-space and focuses onto a  $P$  wave at  $z_F$  at  $\tau = 0$ , hence

$$\begin{pmatrix} \delta(\tau) \\ 0 \end{pmatrix} = \int_{-\infty}^{\tau} \mathbf{T}(p, z_F, z_T, \tau - \tau') \mathbf{f}_p^+(p, z_T, \tau') d\tau', \quad (9)$$

where  $\mathbf{T}(p, z_F, z_T, \tau)$  is the transmission response matrix of the reference medium [partitioned in a similar way as  $\mathbf{R}$  and  $\mathbf{G}^{\pm,+}$  in Eqs. (6) and (8)]. Similar as  $\mathbf{u}^+(p, z, \tau)$  in Eq. (4),  $\mathbf{f}_p^+(p, z_T, \tau)$  is a vector containing downgoing  $P$  and  $S$  waves. According to Eq. (9), these waves are shaped such that their combined responses at  $z_F$  consist of only a downgoing  $P$  wave, equal to  $\delta(\tau)$ . We define a second focusing wavefield vector  $\mathbf{f}_s^+(p, z, \tau)$ , which focuses onto an  $S$  wave at  $z_F$  at  $\tau = 0$ , according to

$$\begin{pmatrix} 0 \\ \delta(\tau) \end{pmatrix} = \int_{-\infty}^{\tau} \mathbf{T}(p, z_F, z_T, \tau - \tau') \mathbf{f}_s^+(p, z_T, \tau') d\tau'. \quad (10)$$

Here  $\mathbf{f}_s^+(p, z_T, \tau)$  contains downgoing  $P$  and  $S$  waves, shaped such that their combined responses at  $z_F$  consist of only a downgoing  $S$  wave, equal to  $\delta(\tau)$ . Equations (9) and (10) can be captured by one equation by combining the vectors on the left- and right-hand sides into matrices, according to

$$\mathbf{I}\delta(\tau) = \int_{-\infty}^{\tau} \mathbf{T}(p, z_F, z_T, \tau - \tau') \mathbf{F}_1^+(p, z_T, z_F, \tau') d\tau', \quad (11)$$

where  $\mathbf{I}$  is the identity matrix and  $\mathbf{F}_1^+(p, z_T, z_F, \tau)$  is a focusing wavefield matrix, of which the columns are formed by the vectors  $\mathbf{f}_p^+$  and  $\mathbf{f}_s^+$ . Note that we included the focal depth  $z_F$  in the argument list of  $\mathbf{F}_1^+$ . The upgoing response at  $z_T$  to the focusing matrix is defined as  $\mathbf{F}_1^-(p, z_T, z_F, \tau)$ . These matrices are partitioned similar as  $\mathbf{R}$  and  $\mathbf{G}^{\pm,+}$  in Eqs. (6) and (8), hence

$$\mathbf{F}_1^{\pm}(p, z_T, z_F, \tau) = \begin{pmatrix} f_{P,P}^{\pm} & f_{P,S}^{\pm} \\ f_{S,P}^{\pm} & f_{S,S}^{\pm} \end{pmatrix}(p, z_T, z_F, \tau). \quad (12)$$

Here the first subscript refers to the wave type at  $z_T$ , whereas the second subscript denotes the type of wave onto which is focused at  $z_F$ .

In Appendix B we derive the following relations between the Green's matrices in the actual medium, the reflection response matrix at the top boundary of the actual medium, and the focusing matrices in the reference medium:

$$\begin{aligned} \mathbf{G}^{-,+}(p, z_T, z_F, \tau) + \mathbf{F}_1^-(p, z_T, z_F, \tau) \\ = \int_{-\infty}^{\tau} \mathbf{R}(p, z_T, \tau - \tau') \mathbf{F}_1^+(p, z_T, z_F, \tau') d\tau', \end{aligned} \quad (13)$$

and

$$\begin{aligned} -\mathbf{G}^{-,-}(p, z_T, z_F, \tau) - \mathbf{F}_1^+(-p, z_T, z_F, -\tau) \\ = - \int_{-\infty}^{\tau} \mathbf{R}(p, z_T, \tau - \tau') \mathbf{F}_1^-(-p, z_T, z_F, -\tau') d\tau'. \end{aligned} \quad (14)$$

Here  $\mathbf{G}^{-,+}(p, z_T, z_F, \tau)$  is the Green's matrix, describing the upward propagating  $P$  and  $S$  fields at  $z_T$ , in response to downward radiating virtual  $P$  and  $S$  sources at  $z_F$ . Similarly,  $-\mathbf{G}^{-,-}(p, z_T, z_F, \tau)$  describes the upward propagating fields at  $z_T$ , in response to upward radiating virtual sources at  $z_F$

[the minus sign in  $-\mathbf{G}^{-,-}(p, z_T, z_F, \tau)$  is introduced here to compensate for the minus sign in the reciprocity relation  $-\mathbf{G}^{-,-}(p, z_T, z_F, \tau) = \{\mathbf{G}^{+,+}(-p, z_F, z_T, \tau)\}'$  (superscript  $t$  denotes transposition)]. Equation (14) holds under the assumption that the waves are propagating (i.e., nonevanescant) at  $z = z_T$  and  $z = z_F$  [this condition does not apply to Eq. (13)]. Note that  $\mathbf{G}^{-,+}$  and  $-\mathbf{G}^{-,-}$  together form the total response to virtual sources at  $z_F$ , similar as in the  $\tau > 0$  parts of Figs. 4(a) and 4(b). Hence, the single-sided representation Eqs. (13) and (14) provide the basis for an alternative to the two-sided time-reversal method. The reflection response  $\mathbf{R}(p, z_T, \tau)$  in these representations is obtained from measurements at the top boundary  $z_T$  only. Once the focusing functions  $\mathbf{F}_1^+$  and  $\mathbf{F}_1^-$  are known, the Green's functions follow from Eqs. (13) and (14).

#### IV. SINGLE-SIDED MARCHENKO FOCUSING: THEORY

Equations (13) and (14) can be seen as a system of two matrix equations for four unknowns (the two focusing matrices and the two Green's matrices). Because of causality, the Green's functions are nonzero only after the arrival time of the direct waves. The focusing functions are also nonzero only in specific time intervals. If there were no overlap of the time intervals in which the Green's functions and the focusing functions are nonzero, then the system of equations could be solved first for the two focusing functions in their time intervals, after which the Green's functions would follow from straightforward substitution of the focusing functions into Eqs. (13) and (14). However, unfortunately the time intervals of the focusing functions and Green's functions do partly overlap. In the following we discuss one possible route to resolve the focusing functions from Eqs. (13) and (14) by making a number of assumptions. It remains to be investigated whether a more general approach is possible.

We start by defining the arrival time of the direct wave of  $G_{X,Y}^-(p, z_T, z_F, \tau)$  as  $\tau_{XY}^d$ . Because  $P$  waves travel faster than  $S$  waves,  $\tau_{PP}^d$  is the smallest direct arrival time. The direct wave of the Green's function  $G_{P,P}^-(p, z_T, z_F, \tau)$  propagates as a  $P$  wave in all layers between  $z_F$  and  $z_T$ . This is different for the other components of the Green's matrix. For example, the first arriving wave of  $G_{S,S}^-(p, z_T, z_F, \tau)$  propagates as an  $S$  wave through the first and last layer and as a  $P$  wave in all intermediate layers, etc. We define a time-window matrix  $\mathbf{W}(p, \tau)$ , according to

$$\mathbf{W}(p, \tau) = \begin{pmatrix} H(\tau_{PP}^d - \epsilon - \tau) & H(\tau_{PS}^d - \epsilon - \tau) \\ H(\tau_{SP}^d - \epsilon - \tau) & H(\tau_{SS}^d - \epsilon - \tau) \end{pmatrix}, \quad (15)$$

where  $H(\tau)$  is the Heaviside step function and  $\epsilon$  a small positive constant. Note that  $H(\tau_{XY}^d - \epsilon - \tau)$  equals zero for  $\tau \geq \tau_{XY}^d(p)$ , that is, at and after the first arrival at  $\tau_{XY}^d(p)$ . The Green's function  $G_{X,Y}^-(p, z_T, z_F, \tau)$  is by definition zero before the first arrival. Hence, the product  $H(\tau_{XY}^d(p) - \epsilon - \tau) G_{X,Y}^-(p, z_T, z_F, \tau)$  is zero for all  $\tau$ . In matrix notation this becomes

$$\mathbf{W}(p, \tau) \circ \mathbf{G}^{-,-}(p, z_T, z_F, \tau) = \mathbf{O}, \quad (16)$$

where  $\mathbf{O}$  is the null matrix and  $\circ$  denotes Hadamard matrix multiplication (i.e., element-wise multiplication). The first

arrival in  $G_{X,Y}^{-,+}(p, z_T, z_F, \tau)$  arrives at or after  $\tau_{XY}^d(p)$ , hence, we also have

$$\mathbf{W}(p, \tau) \circ \mathbf{G}^{-,+}(p, z_T, z_F, \tau) = \mathbf{O}. \quad (17)$$

Applying the time-window matrix  $\mathbf{W}(p, \tau)$  via a Hadamard multiplication to both sides of Eqs. (13) and (14), using Eqs. (16) and (17), yields

$$\begin{aligned} & \mathbf{W}(p, \tau) \circ \mathbf{F}_1^-(p, z_T, z_F, \tau) \\ &= \mathbf{W}(p, \tau) \circ \int_{-\infty}^{\tau} \mathbf{R}(p, z_T, \tau - \tau') \mathbf{F}_1^+(p, z_T, z_F, \tau') d\tau', \end{aligned} \quad (18)$$

and

$$\begin{aligned} & \mathbf{W}(p, \tau) \circ \mathbf{F}_1^+(-p, z_T, z_F, -\tau) \\ &= \mathbf{W}(p, \tau) \circ \int_{-\infty}^{\tau} \mathbf{R}(p, z_T, \tau - \tau') \mathbf{F}_1^-(-p, z_T, z_F, -\tau') d\tau'. \end{aligned} \quad (19)$$

This system of equations is not yet suited to resolve the focusing functions  $\mathbf{F}_1^+$  and  $\mathbf{F}_1^-$ , because parts of these functions may be cut off by the window functions on the left-hand sides.

In the scalar version of Eq. (18), the left-hand side  $W(p, \tau) f_1^-(p, z_T, z_F, \tau)$  is equal to  $f_1^-(p, z_T, z_F, \tau)$ , because the latter function is nonzero only before the direct arrival. In other words, the time-interval in which this focusing function resides is complementary to the time interval in which the Green's function is nonzero. In the elastodynamic case,  $\mathbf{W}(p, \tau) \circ \mathbf{F}_1^-(p, z_T, z_F, \tau)$  is only equal to  $\mathbf{F}_1^-(p, z_T, z_F, \tau)$  when the focal point (at depth  $z_F$ ) is not too close to the interface directly above it. In the following we will assume that this condition is obeyed, hence, Eq. (18) thus becomes

$$\begin{aligned} & \mathbf{F}_1^-(p, z_T, z_F, \tau) \\ &= \mathbf{W}(p, \tau) \circ \int_{-\infty}^{\tau} \mathbf{R}(p, z_T, \tau - \tau') \mathbf{F}_1^+(p, z_T, z_F, \tau') d\tau'. \end{aligned} \quad (20)$$

In the scalar version of Eq. (19), the left-hand side reads  $W(p, \tau) f_1^+(-p, z_T, z_F, -\tau)$ . Here the window function cuts off precisely one event at  $\tau^d(p)$ , the arrival time of the direct wave of the scalar Green's function [24]. We generalize this for the elastodynamic situation. First note that, according to Eq. (11), the focusing matrix  $\mathbf{F}_1^+(p, z_T, z_F, \tau)$  is the inverse of the transmission response matrix  $\mathbf{T}(p, z_F, z_T, \tau)$  of the reference medium (which, between  $z_T$  and  $z_F$ , is equal to the actual medium). Hence,

$$\mathbf{F}_1^+(p, z_T, z_F, \tau) = \mathbf{T}^{\text{inv}}(p, z_F, z_T, \tau). \quad (21)$$

We rewrite the right-hand side as a superposition of two terms, according to

$$\mathbf{F}_1^+(p, z_T, z_F, \tau) = \mathbf{T}_{\text{fs}}^{\text{inv}}(p, z_F, z_T, \tau) + \mathbf{M}^+(p, z_T, z_F, \tau), \quad (22)$$

where  $\mathbf{T}_{\text{fs}}^{\text{inv}}(p, z_F, z_T, \tau)$  is the inverse of the ‘‘forward-scattering’’ transmission response matrix  $\mathbf{T}_{\text{fs}}(p, z_F, z_T, \tau)$ , i.e., the part of the transmission response that includes direct and forward converted waves, but no internal multiples.  $\mathbf{M}^+(p, z_T, z_F, \tau)$  represents the scattering coda [i.e., everything that is not included in  $\mathbf{T}_{\text{fs}}^{\text{inv}}(p, z_F, z_T, \tau)$ ]. Our previous analysis [23] shows that the window function in Eq. (19) cuts off

the direct and forward converted waves, hence

$$\mathbf{W}(p, \tau) \circ \mathbf{F}_1^+(-p, z_T, z_F, -\tau) = \mathbf{M}^+(-p, z_T, z_F, -\tau). \quad (23)$$

Equation (19) thus becomes

$$\begin{aligned} & \mathbf{M}^+(-p, z_T, z_F, -\tau) \\ &= \mathbf{W}(p, \tau) \circ \int_{-\infty}^{\tau} \mathbf{R}(p, z_T, \tau - \tau') \mathbf{F}_1^-(-p, z_T, z_F, -\tau') d\tau'. \end{aligned} \quad (24)$$

Using Eq. (22), Eq. (20) becomes

$$\begin{aligned} & \mathbf{F}_1^-(p, z_T, z_F, \tau) \\ &= \mathbf{F}_{1,0}^-(p, z_T, z_F, \tau) \\ &+ \mathbf{W}(p, \tau) \circ \int_{-\infty}^{\tau} \mathbf{R}(p, z_T, \tau - \tau') \mathbf{M}^+(p, z_T, z_F, \tau') d\tau', \end{aligned} \quad (25)$$

with

$$\begin{aligned} & \mathbf{F}_{1,0}^-(p, z_T, z_F, \tau) \\ &= \mathbf{W}(p, \tau) \circ \int_{-\infty}^{\tau} \mathbf{R}(p, z_T, \tau - \tau') \mathbf{T}_{\text{fs}}^{\text{inv}}(p, z_F, z_T, \tau') d\tau'. \end{aligned} \quad (26)$$

Equations (24) and (25) form a system of elastodynamic Marchenko equations for the focusing matrix  $\mathbf{F}_1^-(p, z_T, z_F, \tau)$  and the scattering coda  $\mathbf{M}^+(p, z_T, z_F, \tau)$  of the focusing matrix  $\mathbf{F}_1^+(p, z_T, z_F, \tau)$ . These equations can be solved by the following iterative Marchenko scheme:

$$\begin{aligned} & \mathbf{M}_k^+(p, z_T, z_F, -\tau) \\ &= \mathbf{W}(p, \tau) \circ \int_{-\infty}^{\tau} \mathbf{R}(p, z_T, \tau - \tau') \mathbf{F}_{1,k}^-(p, z_T, z_F, -\tau') d\tau' \end{aligned} \quad (27)$$

and

$$\begin{aligned} & \mathbf{F}_{1,k+1}^-(p, z_T, z_F, \tau) \\ &= \mathbf{F}_{1,0}^-(p, z_T, z_F, \tau) \\ &+ \mathbf{W}(p, \tau) \circ \int_{-\infty}^{\tau} \mathbf{R}(p, z_T, \tau - \tau') \mathbf{M}_k^+(p, z_T, z_F, \tau') d\tau', \end{aligned} \quad (28)$$

with  $\mathbf{F}_{1,0}^-(p, z_T, z_F, \tau)$  again defined by Eq. (26). The scheme starts with  $k = 0$ .

Assuming the reflection response matrix  $\mathbf{R}(p, z_T, \tau)$  is available from single-sided reflection experiments at the top boundary  $z_T$ , and assuming an estimate of the forward-scattering transmission response matrix  $\mathbf{T}_{\text{fs}}(p, z_F, z_T, \tau)$  is available to initiate the scheme [Eq. (26)], this iterative scheme will give the focusing matrix  $\mathbf{F}_1^-(p, z_T, z_F, \tau)$  and the scattering coda  $\mathbf{M}^+(p, z_T, z_F, \tau)$  of the focusing matrix  $\mathbf{F}_1^+(p, z_T, z_F, \tau)$ . Substituting the results into Eqs. (22), (13), and (14) finally gives the Green's matrices  $\mathbf{G}^{-,+}(p, z_T, z_F, \tau)$  and  $-\mathbf{G}^{-,-}(p, z_T, z_F, \tau)$ .

Note that until now we have assumed that the half-space above the top boundary  $z_T$  is homogeneous. In other words, the boundary at  $z_T$  is considered to be a transparent boundary.

In many cases the top boundary is a free boundary. This free boundary acts as a total reflector for waves coming from below and gives rise to so-called surface-related multiple reflections and conversions (to be distinguished from internal multiple reflections and conversions). Two approaches can be followed to deal with these surface-related effects. One approach is to eliminate the surface-related multiple reflections and conversions from the reflection response by a well-established process [25–27], after which the response is the same as in a medium with a transparent top boundary  $z_T$  and a homogeneous upper half-space. Hence, after this process the conditions are as described at the beginning of Sec. III, which implies that the iterative method described in this section can be followed without further modifications. Another approach is to modify the representations in Sec. III to account for the free-surface boundary conditions and adjust the iterative scheme in this section accordingly. This approach is pursued for acoustic waves in Ref. [28]. For elastodynamic waves this approach is currently under investigation. For the numerical example in the next section it is assumed that the top boundary  $z_T$  is transparent, so that the scheme discussed in this section can be applied without modification.

#### V. SINGLE-SIDED MARCHENKO FOCUSING: NUMERICAL EXAMPLE

We illustrate the iterative Marchenko scheme for the horizontally layered medium of Fig. 2. We model the reflection response matrix  $\mathbf{R}(p, z_T, \tau)$  via the  $(p, z, \omega)$  domain for a single rayparameter  $p = 0.0002$  s/m [17]. This represents the elastodynamic reflection data, measured at the surface  $z_T = 0$ . Furthermore, we model the “forward-scattering” transmission response matrix  $\mathbf{T}_{fs}(p, z_F, z_T, \tau)$  of the medium between  $z_T = 0$  and  $z_F = 1800$ ; multiples are excluded in this modeling process. In practice this transmission response matrix could be modeled in an estimated model of the medium between  $z_T$  and  $z_F$ . The sensitivity with respect to errors in this model needs to be further investigated. It is expected that the requirements for a model that explains only forward scattering are less severe than the requirements for a model that explains forward and backward scattered multiple reflections. Here we assume that the medium between  $z_T$  and  $z_F$  is known, so that we can investigate the performance of the elastodynamic Marchenko scheme under ideal circumstances.

The  $\tau < 0$  part of the top trace in Fig. 6(a) shows the focusing function  $\mathbf{F}_1^+(p, z_T, z_F, \tau)$  obtained from  $\mathbf{R}(p, z_T, \tau)$  and  $\mathbf{T}_{fs}(p, z_F, z_T, \tau)$  after four iterations of the Marchenko scheme [Eqs. (27) and (28)]. To be more specific, it shows the superposition of the elements  $f_{p,P}^+(p, z_T, z_F, \tau)$  and  $f_{s,P}^+(p, z_T, z_F, \tau)$  in the left column of  $\mathbf{F}_1^+$ , i.e., the downward propagating  $P$  and  $S$  waves at  $z_T = 0$ , giving rise to a  $P$ -wave focus at  $z_F$ . These focusing functions are emitted into the real medium (actually, in this numerical experiment we model the response of the medium to these focusing functions). Figure 6(a) shows how this complex wave field propagates through the medium and, unlike in Fig. 5(a), causes a well-defined  $P$ -wave focus at  $\tau = 0$  and  $z_F = 1800$ . The focal point acts as a virtual source for downgoing  $P$  waves, which, after propagation and scattering, reach the top surface  $z_T$  in the form of upgoing  $P$  and  $S$  waves [the left column of  $\mathbf{G}^{-+}(p, z_T, z_F, \tau)$  in Eq. (13)].

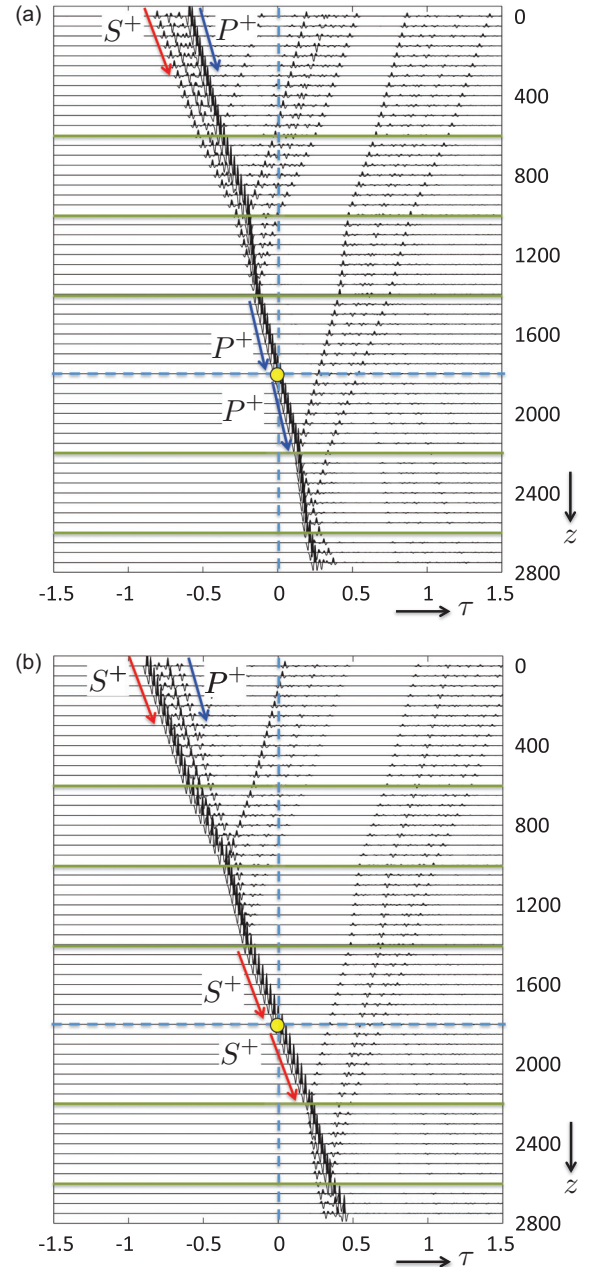


FIG. 6. (Color online) Illumination of actual medium from above by  $\mathbf{F}_1^+$ .

Figure 6(b) shows a similar exercise, this time with the right column of  $\mathbf{F}_1^+$  emitted from  $z_T$  into the medium. This yields an  $S$ -wave focus at  $z_F = 1800$ , which acts as a virtual source for downgoing  $S$ -waves. After propagation and scattering, this finally results in upgoing  $P$  and  $S$  waves at the top surface  $z_T$  [the right column of  $\mathbf{G}^{-+}(p, z_T, z_F, \tau)$  in Eq. (13)].

Compared with the virtual  $P$  and  $S$  wave sources obtained with the two-sided time-reversal method (Fig. 4), the results in Fig. 6 still lack virtual sources for upgoing  $P$  and  $S$  waves. Equation (14) suggests to emit the time-reversal of  $-\mathbf{F}_1^-$  (for opposite rayparameter) from  $z_T$  into the medium, which gives  $-\mathbf{G}^{-}(p, z_T, z_F, \tau)$ , i.e., the response to a virtual source for upgoing waves at  $z_F$ . Figure 7 shows the effect of emitting

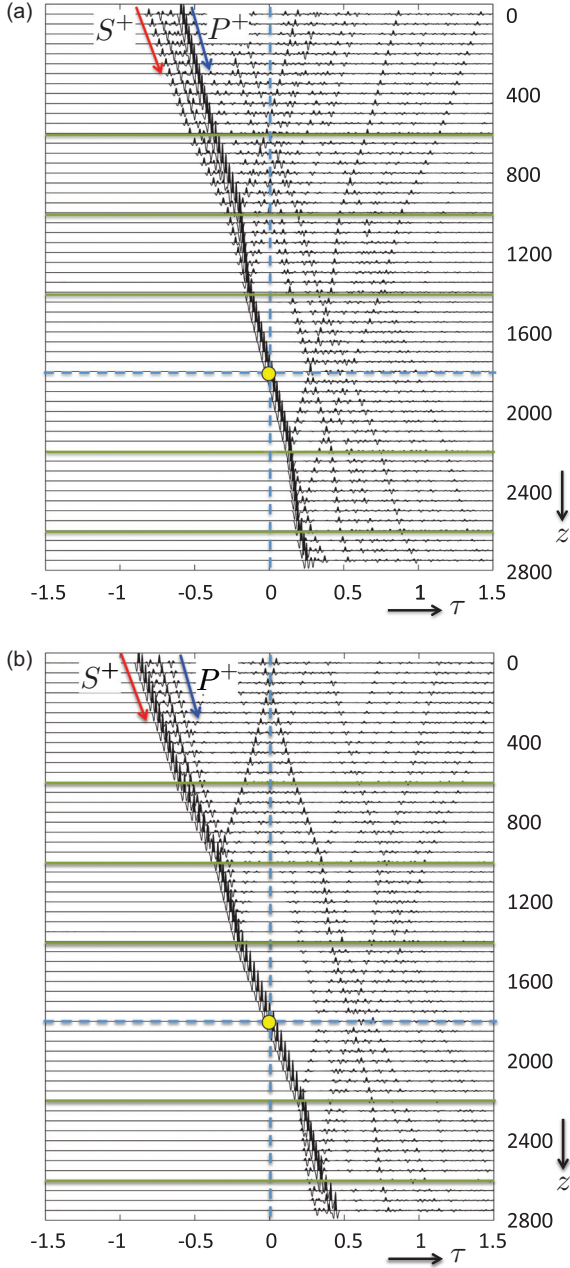


FIG. 7. (Color online) Illumination from above by  $\mathbf{F}_1^+$  and the time-reversal of  $-\mathbf{F}_1^-$ .

the superposition of  $\mathbf{F}_1^+$  and the time-reversal of  $-\mathbf{F}_1^-$  into the medium. The interpretation of this figure is difficult because of the many superposed functions. To simplify this we follow a similar procedure as Brogini and Snieder [11] proposed for the scalar case. From Eqs. (13) and (14) it follows that the trace at  $z_T$  in Fig. 7 consists of (in simplified notation)

$$\mathbf{H}(p, \tau) = \mathbf{F}_1^+(p, \tau) + \mathbf{F}_1^-(p, \tau) + \mathbf{G}^{-,+}(p, \tau) - \mathbf{F}_1^-(-p, -\tau) - \mathbf{F}_1^+(-p, -\tau) - \mathbf{G}^{-,-}(p, \tau). \quad (29)$$

Note that this expression contains the illuminating fields on the right-hand sides as well as their responses on the left-hand sides of Eqs. (13) and (14). If we combine  $\mathbf{H}(p, \tau)$  with its

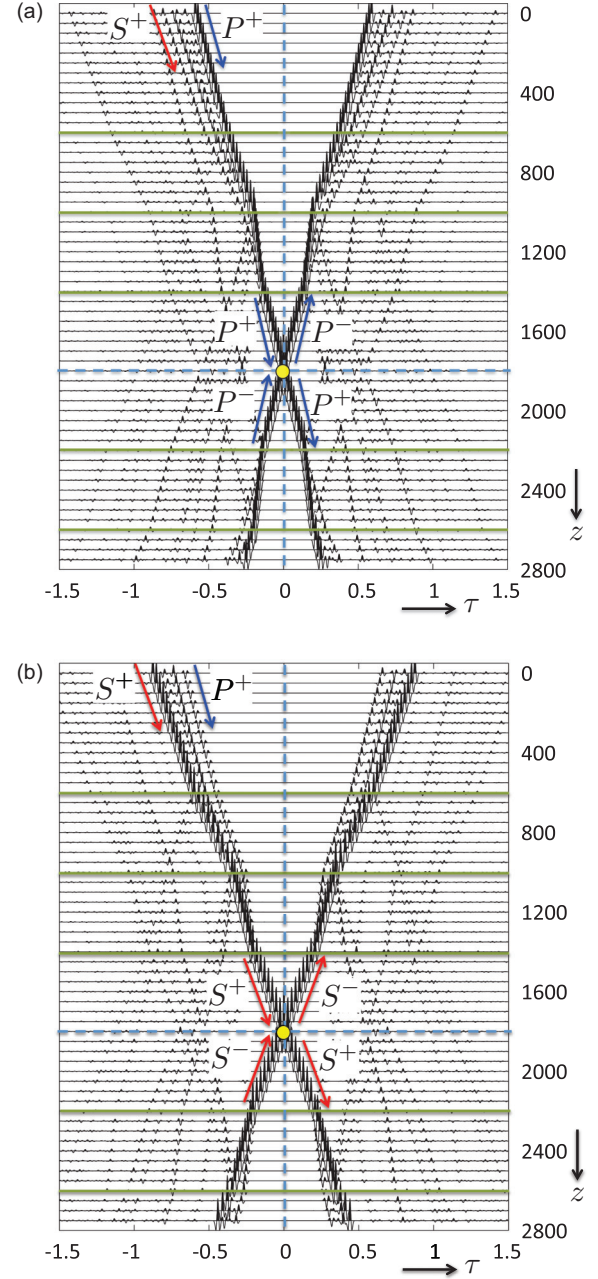


FIG. 8. (Color online) Superposition of Fig. 7 and its time-reversal.

time-reversal (for opposite rayparameter), we obtain

$$\mathbf{H}(p, \tau) + \mathbf{H}(-p, -\tau) = \mathbf{G}(p, \tau) + \mathbf{G}(-p, -\tau), \quad (30)$$

with

$$\mathbf{G}(p, \tau) = \mathbf{G}^{-,+}(p, z_T, z_F, \tau) - \mathbf{G}^{-,-}(p, z_T, z_F, \tau). \quad (31)$$

Hence, with this simple operation the focusing functions are removed, leaving the Green's function and its time-reversal. Applying this operation to all traces in Fig. 7(a) yields Fig. 8(a). Note that the  $\tau > 0$  part clearly shows the response to a virtual source at  $z_F$ , radiating downgoing and upgoing  $P$  waves into the medium. Applying the same process to all traces in Fig. 7(b)

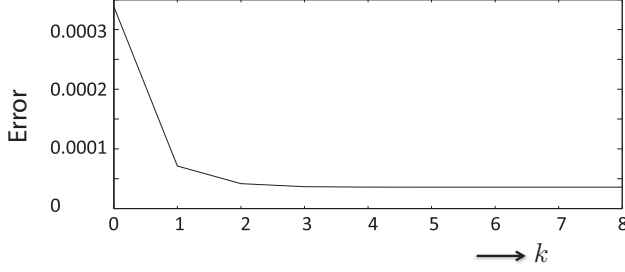


FIG. 9. Error as a function of the iteration number.

yields a virtual source at  $z_F$  for downgoing and upgoing  $S$  waves, Fig. 8(b).

Figure 8 is indistinguishable from Fig. 4. However, whereas Fig. 4 was obtained by emitting time-reversed fields from two sides into the medium, Fig. 8 has been obtained from the reflection response matrix  $\mathbf{R}(p, z_T, \tau)$  at the top surface and the focusing functions  $\mathbf{F}_1^+$  and  $\mathbf{F}_1^-$  which, in turn, have been obtained from  $\mathbf{R}(p, z_T, \tau)$  and the forward-scattering transmission response matrix  $\mathbf{T}_{fs}(p, z_F, z_T, \tau)$ .

We conclude this section by evaluating the error as a function of the iteration number. We compute the averaged absolute difference between the retrieved and the directly modeled Green's function at  $z_T$  (averaged over time and the components of the Green's matrix). The error is defined as this averaged difference, divided by the absolute maximum value of the directly modeled Green's function. Figure 9 shows this error as a function of the iteration number  $k$ . Note that the scheme converges rapidly. After four iterations no further improvement is obtained.

## VI. EXTENSION TO 3D INHOMOGENEOUS MEDIA

We briefly indicate the steps needed to extend the method discussed here for 3D inhomogeneous media. In Ref. [23] we derived the following 3D version of the single-sided Green's function representation

$$\mathbf{G}^{-,+}(\mathbf{x}_T'', \mathbf{x}_F'', t) + \mathbf{F}_1^-(\mathbf{x}_T'', \mathbf{x}_F'', t) = \int_{\partial\mathbb{D}_T} d\mathbf{x}_T \int_{-\infty}^t \mathbf{R}(\mathbf{x}_T'', \mathbf{x}_T, t-t') \mathbf{F}_1^+(\mathbf{x}_T, \mathbf{x}_F', t') dt' \quad (32)$$

and

$$-\mathbf{G}^{-,-}(\mathbf{x}_T'', \mathbf{x}_F'', t) - \mathbf{F}_1^+(\mathbf{x}_T'', \mathbf{x}_F'', -t) = - \int_{\partial\mathbb{D}_T} d\mathbf{x}_T \int_{-\infty}^t \mathbf{R}(\mathbf{x}_T'', \mathbf{x}_T, t-t') \mathbf{F}_1^-(\mathbf{x}_T, \mathbf{x}_F', -t') dt'. \quad (33)$$

Here  $\partial\mathbb{D}_T$  denotes the top boundary  $z = z_T$  of a 3D inhomogeneous medium below a homogeneous half-space. Coordinates at this top boundary are denoted as  $\mathbf{x}_T = (x, y, z_T)$ . Similarly,  $\mathbf{x}_F' = (x', y', z_F)$  denotes the coordinates of a focal point at depth  $z = z_F$ .  $\mathbf{R}(\mathbf{x}_T'', \mathbf{x}_T, t)$  is the 3D reflection response matrix at  $z_T$ . It is a  $3 \times 3$  matrix, in which the different columns correspond to the different sources at  $\mathbf{x}_T$  for downgoing  $P$  and  $S$  waves (the latter for two different types of polarization). The different elements within the columns correspond to the

different upgoing  $P$  and  $S$  waves at  $\mathbf{x}_T''$ .  $\mathbf{F}_1^\pm(\mathbf{x}_T, \mathbf{x}_F', t)$  is a similarly organized  $3 \times 3$  matrix, containing the downgoing (+) and upgoing (-) parts of the focusing functions at  $\mathbf{x}_T$ , which focus to  $P$  and  $S$  waves at  $\mathbf{x}_F'$  (the first column focuses to a  $P$  wave, the second and third columns focus to two types of  $S$  waves).  $\mathbf{G}^{-,\pm}(\mathbf{x}_T'', \mathbf{x}_F'', t)$  is a  $3 \times 3$  Green's matrix. Here the different columns correspond to different types of virtual sources at  $\mathbf{x}_F'$  for downgoing (+) and upgoing (-) waves, of which the responses are observed as upgoing waves at  $\mathbf{x}_T''$ . The underlying assumption of Eqs. (32) and (33) is that the medium is lossless. Moreover, for Eq. (33) it is assumed that evanescent waves can be neglected at  $z = z_T$  and  $z = z_F$ .

Similar as in Eqs. (13) and (14), the Green's functions and focusing functions on the left-hand sides of Eqs. (32) and (33) partly overlap each other in the time domain. Here we discuss one possible way to deal with this overlap by removing the Green's functions from these equations and solve the remaining system of equations for the focusing functions. To this end, a  $3 \times 3$  window matrix  $\mathbf{W}(\mathbf{x}_T'', \mathbf{x}_F'', t)$  is defined, containing Heaviside step functions  $H[t_{XY}^d(\mathbf{x}_T'', \mathbf{x}_F'') - \epsilon - t]$ , where  $t_{XY}^d(\mathbf{x}_T'', \mathbf{x}_F'')$  is the traveltime of the first arrival of  $G_{X,Y}^{-,+}(\mathbf{x}_T'', \mathbf{x}_F'', t)$ . Applying this window matrix to the Green's matrices gives

$$\mathbf{W}(\mathbf{x}_T'', \mathbf{x}_F'', t) \circ \mathbf{G}^{-,\pm}(\mathbf{x}_T'', \mathbf{x}_F'', t) = \mathbf{O}. \quad (34)$$

Moreover, assuming the focal point is not too close to the interface directly above it, we have

$$\mathbf{W}(\mathbf{x}_T'', \mathbf{x}_F'', t) \circ \mathbf{F}_1^-(\mathbf{x}_T'', \mathbf{x}_F'', t) = \mathbf{F}_1^-(\mathbf{x}_T'', \mathbf{x}_F'', t). \quad (35)$$

Analogous to Eq. (22), we write  $\mathbf{F}_1^+(\mathbf{x}_T'', \mathbf{x}_F'', t)$  as

$$\mathbf{F}_1^+(\mathbf{x}_T'', \mathbf{x}_F'', t) = \mathbf{T}_{fs}^{\text{inv}}(\mathbf{x}_F', \mathbf{x}_T'', t) + \mathbf{M}^+(\mathbf{x}_T'', \mathbf{x}_F'', t), \quad (36)$$

where  $\mathbf{T}_{fs}^{\text{inv}}(\mathbf{x}_F', \mathbf{x}_T'', t)$  is the inverse of the forward-scattering transmission response matrix  $\mathbf{T}_{fs}(\mathbf{x}_F', \mathbf{x}_T'', t)$ . The latter matrix contains not only the direct and forward converted waves of the full transmission response matrix, but also triplicated waves in case of multipathing [13].  $\mathbf{M}^+(\mathbf{x}_T'', \mathbf{x}_F'', t)$  in Eq. (36) represents all other scattering events, which are not included in  $\mathbf{T}_{fs}^{\text{inv}}(\mathbf{x}_F', \mathbf{x}_T'', t)$ . Applying the window matrix to the time-reversal of  $\mathbf{F}_1^+(\mathbf{x}_T'', \mathbf{x}_F'', t)$  gives

$$\mathbf{W}(\mathbf{x}_T'', \mathbf{x}_F'', t) \circ \mathbf{F}_1^+(\mathbf{x}_T'', \mathbf{x}_F'', -t) = \mathbf{M}^+(\mathbf{x}_T'', \mathbf{x}_F'', -t). \quad (37)$$

Keep in mind that, like in the 3D scalar case, Eqs. (34)–(37) are not guaranteed to hold under all circumstances. In the following we only consider situations for which these equations hold. This is the case, for example, at finite horizontal distances in layered media with moderately curved interfaces [12,13], assuming a focal point not too close to the interface above it.

Applying the window matrix  $\mathbf{W}(\mathbf{x}_T'', \mathbf{x}_F'', t)$  to Eqs. (32) and (33), using equations (34)–(37) and rewriting the resulting equations into an iterative scheme, gives

$$\begin{aligned} & \mathbf{M}_k^+(\mathbf{x}_T'', \mathbf{x}_F'', -t) \\ &= \mathbf{W}(\mathbf{x}_T'', \mathbf{x}_F'', t) \circ \int_{\partial\mathbb{D}_T} d\mathbf{x}_T \int_{-\infty}^t \mathbf{R}(\mathbf{x}_T'', \mathbf{x}_T, t-t') \\ & \quad \times \mathbf{F}_{1,k}^-(\mathbf{x}_T, \mathbf{x}_F', -t') dt' \end{aligned} \quad (38)$$

and

$$\begin{aligned} \mathbf{F}_{1,k+1}^-(\mathbf{x}_T'', \mathbf{x}_F', t) &= \mathbf{F}_{1,0}^-(\mathbf{x}_T'', \mathbf{x}_F', t) + \mathbf{W}(\mathbf{x}_T'', \mathbf{x}_F', t) \circ \int_{\partial\mathbb{D}_T} d\mathbf{x}_T \\ &\quad \times \int_{-\infty}^t \mathbf{R}(\mathbf{x}_T'', \mathbf{x}_T, t - t') \mathbf{M}_k^+(\mathbf{x}_T, \mathbf{x}_F', t') dt', \end{aligned} \quad (39)$$

with

$$\begin{aligned} \mathbf{F}_{1,0}^-(\mathbf{x}_T'', \mathbf{x}_F', t) &= \mathbf{W}(\mathbf{x}_T'', \mathbf{x}_F', t) \circ \int_{\partial\mathbb{D}_T} d\mathbf{x}_T \int_{-\infty}^t \mathbf{R}(\mathbf{x}_T'', \mathbf{x}_T, t - t') \\ &\quad \times \mathbf{T}_{fs}^{\text{inv}}(\mathbf{x}_F', \mathbf{x}_T', t') dt'. \end{aligned} \quad (40)$$

These equations form the 3D version of the single-sided elastodynamic Marchenko scheme. It starts with  $k = 0$ . Assuming the reflection response matrix  $\mathbf{R}(\mathbf{x}_T'', \mathbf{x}_T, t)$  is available from single-sided reflection experiments at the top boundary  $\partial\mathbb{D}_T$ , and assuming an estimate of the forward-scattering transmission response matrix  $\mathbf{T}_{fs}(\mathbf{x}_F', \mathbf{x}_T', t)$  is available, this iterative scheme will give the focusing matrix  $\mathbf{F}_1^-(\mathbf{x}_T'', \mathbf{x}_F', t)$  and the scattering coda  $\mathbf{M}^+(\mathbf{x}_T'', \mathbf{x}_F', t)$  of the focusing matrix  $\mathbf{F}_1^+(\mathbf{x}_T'', \mathbf{x}_F', t)$ . Substituting the results into Eqs. (36), (32), and (33) finally gives the Green's matrices  $\mathbf{G}^{-,+}(\mathbf{x}_T'', \mathbf{x}_F', t)$  and  $-\mathbf{G}^{-,-}(\mathbf{x}_T'', \mathbf{x}_F', t)$ .

The scalar version of this scheme has proven to give accurate Green's functions [12–14]. Da Costa *et al.* [20–22] independently derived a similar 3D elastodynamic Marchenko scheme and illustrated it with 2D numerical examples. For a shallow focal point (situated in the second layer) several arrivals in the Green's functions are well recovered. However, other events are missing and several artefacts (nonexisting arrivals) are generated. In their scheme a direct arrival Green's matrix takes the place of our forward-scattering transmission response matrix  $\mathbf{T}_{fs}(\mathbf{x}_F', \mathbf{x}_T', t)$ . This direct arrival Green's matrix lacks the forward scattering information, necessary for recovering the complete Green's matrices with the iterative scheme. From our initial 1D experiments, presented in Sec. V and in Ref. [23], we expect that the 3D scheme outlined above will lead to an accurate recovery of the elastodynamic Green's matrices. One of the main research issues concerns the investigation of what approximations are allowed in the estimation of the forward-scattering transmission response matrix, needed to initiate the iterative scheme.

## VII. CONCLUDING REMARKS

In the elastodynamic time-reversal method,  $P$  and  $S$  waves are focused at the original source position inside a layered medium by physically emitting time-reversed fields from two sides back into the medium. Our method accomplishes the same type of focusing (compare Fig. 8 with Fig. 4), but does not need a physical source or receiver at the focus location, nor does it need access to the medium from two sides. Our method uses the measured single-sided reflection response and limited information about the transmission response of the medium to derive the focusing functions. Instead of physically emitting these focusing functions into the real medium, we use them in Eqs. (13) and (14) to retrieve the elastodynamic Green's functions at the top boundary, originating from virtual  $P$ - and  $S$ -wave sources inside the medium.

The generalization of the method from horizontally layered media to 3D inhomogeneous media goes along the same lines as for scalar waves [12,13] and has been briefly discussed in Sec. VI. This opens the way to 3D data-driven elastodynamic “Marchenko imaging” of single-sided reflection data, as a generalization of Marchenko imaging of scalar data [14]. Elastodynamic Marchenko imaging will fully employ wave conversion and multiple scattering and is expected to have important applications in nondestructive testing of construction materials and seismological monitoring of geophysical processes inside the Earth.

## APPENDIX A: FLUX-NORMALIZED COMPRESSIONAL AND SHEAR WAVES

For elastodynamic wave fields in a horizontally layered medium we define a wave-field vector  $\mathbf{q}(p, z, \omega)$  as

$$\mathbf{q}(p, z, \omega) = \begin{pmatrix} -\boldsymbol{\tau} \\ \mathbf{v} \end{pmatrix} (p, z, \omega), \quad (A1)$$

where

$$\boldsymbol{\tau} = \begin{pmatrix} \tau_{xz} \\ \tau_{zz} \end{pmatrix} (p, z, \omega) \quad \text{and} \quad \mathbf{v} = \begin{pmatrix} v_x \\ v_z \end{pmatrix} (p, z, \omega) \quad (A2)$$

are the measurable wave-field quantities traction and particle velocity, respectively. We define a second wave-field vector  $\mathbf{u}(p, z, \omega)$  as

$$\mathbf{u}(p, z, \omega) = \begin{pmatrix} \mathbf{u}^+ \\ \mathbf{u}^- \end{pmatrix} (p, z, \omega), \quad (A3)$$

where

$$\mathbf{u}^+ = \begin{pmatrix} P^+ \\ S^+ \end{pmatrix} (p, z, \omega) \quad \text{and} \quad \mathbf{u}^- = \begin{pmatrix} P^- \\ S^- \end{pmatrix} (p, z, \omega) \quad (A4)$$

are the downgoing (+) and upgoing (−) compressional ( $P$ ) and shear ( $S$ ) wave fields. Vectors  $\mathbf{q}(p, z, \omega)$  and  $\mathbf{u}(p, z, \omega)$  are mutually related via a matrix  $\mathbf{L}(p, z)$ , according to

$$\mathbf{q}(p, z, \omega) = \mathbf{L}(p, z) \mathbf{u}(p, z, \omega). \quad (A5)$$

Matrix  $\mathbf{L}(p, z)$  is not uniquely defined. Its definition depends on the chosen normalization of the down- and upgoing compressional and shear waves  $P^\pm$  and  $S^\pm$ . Choosing power-flux normalization for these waves, matrix  $\mathbf{L}(p, z)$  is defined as [29–31]

$$\mathbf{L}(p, z) = \begin{pmatrix} \mathbf{L}_1^+ & \mathbf{L}_1^- \\ \mathbf{L}_2^+ & \mathbf{L}_2^- \end{pmatrix} (p, z), \quad (A6)$$

where

$$\mathbf{L}_1^\pm(p, z) = c_S^2 \left( \frac{\rho}{2} \right)^{\frac{1}{2}} \begin{pmatrix} \pm 2pq_P^{\frac{1}{2}} & -(c_S^{-2} - 2p^2)/q_S^{\frac{1}{2}} \\ (c_S^{-2} - 2p^2)/q_P^{\frac{1}{2}} & \pm 2pq_S^{\frac{1}{2}} \end{pmatrix} \quad (A7)$$

and

$$\mathbf{L}_2^\pm(p, z) = (2\rho)^{-\frac{1}{2}} \begin{pmatrix} p/q_P^{\frac{1}{2}} & \mp q_S^{\frac{1}{2}} \\ \pm q_P^{\frac{1}{2}} & p/q_S^{\frac{1}{2}} \end{pmatrix}. \quad (A8)$$

The vertical  $P$ - and  $S$ -wave slownesses  $q_P(p, z)$  and  $q_S(p, z)$ , respectively, are defined as

$$q_P(p, z) = [c_P^{-2}(z) - p^2]^{\frac{1}{2}} \quad (A9)$$

and

$$q_S(p, z) = [c_S^{-2}(z) - p^2]^{\frac{1}{2}}. \quad (\text{A10})$$

Because of the flux-normalization, matrix  $\mathbf{L}(p, z)$  has a simple inverse

$$\mathbf{L}^{-1}(p, z) = -\mathbf{N}^{-1}\mathbf{L}^t(-p, z)\mathbf{N} = \mathbf{J}^{-1}\mathbf{L}^t(p, z)\mathbf{K} \quad (\text{A11})$$

(superscript  $t$  denotes transposition), with

$$\mathbf{N} = \begin{pmatrix} \mathbf{O} & \mathbf{I} \\ -\mathbf{I} & \mathbf{O} \end{pmatrix}, \quad \mathbf{K} = \begin{pmatrix} \mathbf{O} & \mathbf{I} \\ \mathbf{I} & \mathbf{O} \end{pmatrix}, \quad \mathbf{J} = \begin{pmatrix} \mathbf{I} & \mathbf{O} \\ \mathbf{O} & -\mathbf{I} \end{pmatrix}, \quad (\text{A12})$$

where  $\mathbf{O}$  is the null matrix.

We group the Green's matrices for downgoing and upgoing waves, as introduced in Sec. III, into a single Green's matrix  $\mathbf{G}_I(p, z, z_F, \omega)$ , according to

$$\mathbf{G}_I(p, z, z_F, \omega) = \begin{pmatrix} \mathbf{G}^{+,+} & \mathbf{G}^{+,-} \\ \mathbf{G}^{-,+} & \mathbf{G}^{-,-} \end{pmatrix}(p, z, z_F, \omega). \quad (\text{A13})$$

We define a Green's matrix  $\mathbf{G}_{II}(p, z, z_F, \omega)$  in terms of measurable quantities as follows:

$$\mathbf{G}_{II}(p, z, z_F, \omega) = \begin{pmatrix} \mathbf{G}^{\tau,f} & \mathbf{G}^{\tau,h} \\ \mathbf{G}^{v,f} & \mathbf{G}^{v,h} \end{pmatrix}(p, z, z_F, \omega). \quad (\text{A14})$$

Here the first superscripts ( $\tau$  and  $v$ ) refer to the observed wave field at  $z$  [traction and particle velocity, respectively, similar to Eq. (A1)], whereas the second superscripts ( $f$  and  $h$ ) refer to the source type at  $z_F$  (force and deformation, respectively). Note that the lower left matrix  $\mathbf{G}^{v,f}(p, z, z_F, \omega)$  is the common Green's tensor in terms of particle velocity components in response to force sources. The two Green's matrices are mutually related, according to

$$\mathbf{G}_{II}(p, z, z_F, \omega) = \mathbf{L}(p, z)\mathbf{G}_I(p, z, z_F, \omega)\mathbf{L}^{-1}(p, z_F). \quad (\text{A15})$$

Both Green's matrices obey the reciprocity relation [32]

$$\mathbf{G}(p, z_F, z, \omega) = -\mathbf{N}^{-1}\mathbf{G}^t(-p, z, z_F, \omega)\mathbf{N}, \quad (\text{A16})$$

where  $\mathbf{G}$  stands for  $\mathbf{G}_I$  or  $\mathbf{G}_{II}$ .

## APPENDIX B: DERIVATION OF THE SINGLE-SIDED GREEN'S FUNCTION REPRESENTATION

For elastodynamic wave fields in a horizontally layered lossless and source-free medium, we consider the following two propagation invariants (i.e., quantities independent of  $z$ ) [17,33]:

$$-\tau_A^t(-p, z, \omega)\mathbf{v}_B(p, z, \omega) + \mathbf{v}_A^t(-p, z, \omega)\tau_B(p, z, \omega) \quad (\text{B1})$$

and

$$-\tau_A^\dagger(p, z, \omega)\mathbf{v}_B(p, z, \omega) - \mathbf{v}_A^\dagger(p, z, \omega)\tau_B(p, z, \omega). \quad (\text{B2})$$

Superscript  $\dagger$  denotes transposition and complex conjugation. Subscripts  $A$  and  $B$  refer to two independent solutions of the elastodynamic wave equation for one-and-the-same lossless source-free medium. Using the notation of Appendix A, these propagation invariants can be compactly written as

$\mathbf{q}_A^t(-p, z, \omega)\mathbf{N}\mathbf{q}_B(p, z, \omega)$  and  $\mathbf{q}_A^\dagger(p, z, \omega)\mathbf{K}\mathbf{q}_B(p, z, \omega)$ , respectively. From these propagation invariants, we obtain

$$\mathbf{q}_A^t(-p, z_T, \omega)\mathbf{N}\mathbf{q}_B(p, z_T, \omega) = \mathbf{q}_A^t(-p, z_F, \omega)\mathbf{N}\mathbf{q}_B(p, z_F, \omega) \quad (\text{B3})$$

and

$$\mathbf{q}_A^\dagger(p, z_T, \omega)\mathbf{K}\mathbf{q}_B(p, z_T, \omega) = \mathbf{q}_A^\dagger(p, z_F, \omega)\mathbf{K}\mathbf{q}_B(p, z_F, \omega), \quad (\text{B4})$$

respectively, where  $z_T$  and  $z_F$  denote the top boundary and the focal depth, respectively. Note that for these equations to hold, it is sufficient that only the medium between  $z_T$  and  $z_F$  is lossless, source-free, and the same for wave fields  $\mathbf{q}_A$  and  $\mathbf{q}_B$ . Outside this region, sources may exist and the medium parameters may be different for  $\mathbf{q}_A$  and  $\mathbf{q}_B$ . Substituting Eq. (A5) into Eq. (B3), using Eqs. (A3), (A11), and (A12), gives

$$\begin{aligned} & \{\mathbf{u}_A^+(p, z_T, \omega)\}^t \mathbf{u}_B^-(p, z_T, \omega) - \{\mathbf{u}_A^-(p, z_T, \omega)\}^t \mathbf{u}_B^+(p, z_T, \omega) \\ &= \{\mathbf{u}_A^+(p, z_F, \omega)\}^t \mathbf{u}_B^-(p, z_F, \omega) \\ & \quad - \{\mathbf{u}_A^-(p, z_F, \omega)\}^t \mathbf{u}_B^+(p, z_F, \omega). \end{aligned} \quad (\text{B5})$$

This expression relates downgoing and upgoing wave fields at depth levels  $z_T$  and  $z_F$ . In a similar way we obtain from Eq. (B4)

$$\begin{aligned} & \{\mathbf{u}_A^+(p, z_T, \omega)\}^\dagger \mathbf{u}_B^+(p, z_T, \omega) - \{\mathbf{u}_A^-(p, z_T, \omega)\}^\dagger \mathbf{u}_B^-(p, z_T, \omega) \\ &= \{\mathbf{u}_A^+(p, z_F, \omega)\}^\dagger \mathbf{u}_B^+(p, z_F, \omega) \\ & \quad - \{\mathbf{u}_A^-(p, z_F, \omega)\}^\dagger \mathbf{u}_B^-(p, z_F, \omega), \end{aligned} \quad (\text{B6})$$

assuming  $\mathbf{L}(p, z_T)$  and  $\mathbf{L}(p, z_F)$  are real-valued. This assumption is obeyed when  $q_P(p, z)$  and  $q_S(p, z)$ , defined in Eqs. (A9) and (A10), are real-valued for  $z = z_T$  and  $z = z_F$ , i.e., when  $|p| \leq c_P^{-1}(z) < c_S^{-1}(z)$  for  $z = z_T$  and  $z = z_F$ . In other words, Eq. (B6) holds under the additional assumption that the waves are propagating (i.e., nonevanescant) at  $z = z_T$  and  $z = z_F$ .

We use Eqs. (B5) and (B6) to derive relations between the various quantities defined in Sec. III. To this end, we first transform Eqs. (5), (7), and (11) to the rayparameter-frequency domain, yielding

$$\mathbf{u}^-(p, z_T, \omega) = \mathbf{R}(p, z_T, \omega)\mathbf{u}^+(p, z_T, \omega), \quad (\text{B7})$$

$$\mathbf{u}^\pm(p, z_F, \omega) = \mathbf{G}^{\pm,+}(p, z_F, z_T, \omega)\mathbf{u}^\pm(p, z_T, \omega), \quad (\text{B8})$$

and

$$\mathbf{I} = \mathbf{T}(p, z_F, z_T, \omega)\mathbf{F}_1^\dagger(p, z_T, z_F, \omega), \quad (\text{B9})$$

respectively. For the fields with subscript  $A$  we take the fields in the actual medium. For convenience, we define  $\mathbf{u}_A^+(p, z_T, \omega) = \mathbf{I}$ . Then, according to Eqs. (B7) and (B8), we obtain  $\mathbf{u}_A^-(p, z_T, \omega) = \mathbf{R}(p, z_T, \omega)$  and  $\mathbf{u}_A^\pm(p, z_F, \omega) = \mathbf{G}^{\pm,+}(p, z_F, z_T, \omega)$ . For the fields with subscript  $B$  we take the focusing fields in the reference medium [this is allowed, because between  $z_T$  and  $z_F$  the reference medium is identical to the actual medium; see also the remark below Eq. (B4)]. Hence, we define  $\mathbf{u}_B^+(p, z_T, \omega) = \mathbf{F}_1^\dagger(p, z_T, z_F, \omega)$ . Its response at  $z_T$  is then given by  $\mathbf{u}_B^-(p, z_T, \omega) = \mathbf{F}_1^-(p, z_T, z_F, \omega)$ . According to Eq. (B9) its downgoing response at the focal

depth  $z_F$  is  $\mathbf{u}_B^+(p, z_F, \omega) = \mathbf{I}$ . Since the reference medium is reflection-free below  $z_F$ , we have  $\mathbf{u}_B^-(p, z_F, \omega) = \mathbf{O}$ . Making these substitutions in Eqs. (B5) and (B6), using  $\mathbf{R}(p, z_T, \omega) = \{\mathbf{R}(-p, z_T, \omega)\}^t$  and  $\mathbf{G}^{\pm,+}(p, z_F, z_T, \omega) = \mp \{\mathbf{G}^{\mp,+}(-p, z_T, z_F, \omega)\}^t$  [Eq. (A16)], gives

$$\begin{aligned} & \mathbf{G}^{-,+}(p, z_T, z_F, \omega) + \mathbf{F}_1^-(p, z_T, z_F, \omega) \\ &= \mathbf{R}(p, z_T, \omega) \mathbf{F}_1^+(p, z_T, z_F, \omega) \end{aligned} \quad (\text{B10})$$

and

$$\begin{aligned} & -\mathbf{G}^{-,-}(-p, z_T, z_F, \omega) - \{\mathbf{F}_1^+(p, z_T, z_F, \omega)\}^* \\ &= -\mathbf{R}(-p, z_T, \omega) \{\mathbf{F}_1^-(p, z_T, z_F, \omega)\}^*, \end{aligned} \quad (\text{B11})$$

respectively. Transforming these expressions back to the rayparameter intercept-time domain, replacing  $p$  by  $-p$  in Eq. (B11), gives Eqs. (13) and (14).

- 
- [1] M. Fink, *Phys. Today* **50**, 34 (1997).  
 [2] R. K. Snieder and J. A. Scales, *Phys. Rev. E* **58**, 5668 (1998).  
 [3] M. Fink and C. Prada, *Inverse Probl.* **17**, R1 (2001).  
 [4] G. Lerosey, J. de Rosny, A. Tourin, A. Derode, G. Montaldo, and M. Fink, *Phys. Rev. Lett.* **92**, 193904 (2004).  
 [5] D.-J. van Manen, A. Curtis, and J. O. A. Robertsson, *Geophysics* **71**, SI41 (2006).  
 [6] E. H. Saenger, G. K. Kocur, R. Jud, and M. Torrilhon, *Appl. Math. Model.* **35**, 807 (2011).  
 [7] J. H. Rose, *Phys. Rev. A* **65**, 012707 (2001).  
 [8] J. H. Rose, *Inverse Probl.* **18**, 1923 (2002).  
 [9] V. A. Marchenko, *Dokl. Akad. Nauk SSSR* **104**, 695 (1955).  
 [10] G. L. Lamb, *Elements of Soliton Theory* (John Wiley and Sons, Inc., New York, 1980).  
 [11] F. Broggini and R. Snieder, *Eur. J. Phys.* **33**, 593 (2012).  
 [12] K. Wapenaar, F. Broggini, E. Slob, and R. Snieder, *Phys. Rev. Lett.* **110**, 084301 (2013).  
 [13] K. Wapenaar, J. Thorbecke, J. van der Neut, F. Broggini, E. Slob, and R. Snieder, *J. Acoust. Soc. Am.* **135**, 2847 (2014).  
 [14] K. Wapenaar, J. Thorbecke, J. van der Neut, F. Broggini, E. Slob, and R. Snieder, *Geophysics* **79**, WA39 (2014).  
 [15] F. Broggini, R. Snieder, and K. Wapenaar, *Geophysics* **79**, WA107 (2014).  
 [16] P. L. Stoffa, *Tau-p—A Plane Wave Approach to the Analysis of Seismic Data* (Kluwer Academic Publishers, Dordrecht, 1989).  
 [17] B. L. N. Kennett, *Seismic Wave Propagation in Stratified Media* (Cambridge University Press, Cambridge, 1983).  
 [18] C. Prada, F. Wu, and M. Fink, *J. Acoust. Soc. Am.* **90**, 1119 (1991).  
 [19] C. Prada, S. Manneville, D. Spoliansky, and M. Fink, *J. Acoust. Soc. Am.* **99**, 2067 (1996).  
 [20] C. A. da Costa, M. Ravasi, G. Meles, and A. Curtis, in 76th EAGE Conference and Exhibition (2014), <http://dx.doi.org/10.3997/2214-4609.20141370>.  
 [21] C. da Costa, M. Ravasi, G. Meles, and A. Curtis, *SEG Technical Program Expanded Abstracts* 4603 (2014).  
 [22] C. A. da Costa Filho, M. Ravasi, A. Curtis, and G. A. Meles, *Phys. Rev. E* **90**, 063201 (2014).  
 [23] K. Wapenaar and E. Slob, *Geophys. J. Int.* **199**, 1367 (2014).  
 [24] E. Slob, K. Wapenaar, F. Broggini, and R. Snieder, *Geophysics* **79**, S63 (2014).  
 [25] B. L. N. Kennett, *Geophys. Prosp.* **27**, 584 (1979).  
 [26] C. P. A. Wapenaar, P. Herrmann, D. J. Verschuur, and A. J. Berkhout, *Geophys. Prosp.* **38**, 633 (1990).  
 [27] D. J. Verschuur, A. J. Berkhout, and C. P. A. Wapenaar, *Geophysics* **57**, 1166 (1992).  
 [28] S. Singh, R. Snieder, J. Behura, J. van der Neut, K. Wapenaar, and E. Slob, *SEG Technical Program Expanded Abstracts* 4060 (2014).  
 [29] C. W. Frasier, *Geophysics* **35**, 197 (1970).  
 [30] B. Ursin, *Geophysics* **48**, 1063 (1983).  
 [31] K. Wapenaar, E. Slob, and R. Snieder, *Geophys. Prosp.* **56**, 419 (2008).  
 [32] C. P. A. Wapenaar, *Geophys. J. Int.* **127**, 178 (1996).  
 [33] B. L. N. Kennett, K. Koketsu, and A. J. Haines, *Geophys. J. Int.* **103**, 95 (1990).